PAPER

Global gyrokinetic turbulence simulations of MAST plasmas

To cite this article: S Saarelma *et al* 2012 *Plasma Phys. Control. Fusion* **54** 085012

Plasma Phys. Control. Fusion **54** (2012) 085012 (9pp) doi:10.1088/0741-3335/54/8/085012

Global gyrokinetic turbulence simulations of MAST plasmas

S Saarelma[1], P Hill[3], A Bottino[2], G Colyer[1], A R Field[1], B McMillan[3], A Peeters[4], C M Roach[1] and the MAST team[1]

[1] EURATOM/CCFE Fusion Association, Culham Science Centre, Abingdon, OX14 3DB, UK
[2] MPI für Plasmaphysik, EURATOM Association, D-85748 Garching, Germany
[3] Centre for Fusion, Space and Astrophysics, Warwick University, Coventry CV4 7AL, UK
[4] Department of Physics, University of Bayreuth, D-95440 Bayreuth, Germany

Received 2 February 2012, in final form 3 may 2012
Published 3 July 2012
Online at stacks.iop.org/PPCF/54/085012

Abstract
Electrostatic gyrokinetic analyses are presented for an L-mode discharge with an internal transport barrier, from the spherical tokamak, MAST. Local and global microstability analysis finds similar linear growth rates for ion temperature gradient (ITG) driven modes. When the electron response is assumed to be adiabatic, growth rates are found to be lower than the experimental $\boldsymbol{E} \times \boldsymbol{B}$ flow shearing rate. Including kinetic electrons, without collisions, increases the ITG growth rates above the flow shearing rate, and these modes are found to be linearly unstable in the outer part of the plasma only. In global simulations the flow shear stabilization is found to be asymmetric with respect to the direction of the flow: there is a small destabilizing effect at low flow shear when the flow is in the co-direction.

Global non-linear simulations with kinetic electrons and including the flow shear effects predict turbulent ion heat transport that is well above the neoclassical level in the region outside the internal transport barrier in this MAST plasma. In non-linear simulations we also find turbulence extending from the outer part of the plasma into the linearly stable core region.

(Some figures may appear in colour only in the online journal)

1. Introduction

The anomalous transport from ion scale microturbulence driven by ion temperature gradient (ITG) modes and trapped electron modes (TEMs) in spherical tokamaks (STs) such as MAST and NSTX is thought to be suppressed by sheared $\boldsymbol{E} \times \boldsymbol{B}$ flow in most high confinement mode (H-mode) discharges leaving only the electron scale turbulence driven by the electron temperature gradient (ETG) modes [1–3]. However, in low confinement mode (L-mode) plasmas in NSTX [1], and in L-mode plasmas with internal transport barriers in MAST [5, 6], there are experimental indications that ion scale electrostatic turbulence may still play an important role in transport.

In H-mode ST plasmas with high β electromagnetic ion scale microinstabilities such as kinetic ballooning modes and microtearing modes are found unstable [2, 4]. In L-mode β is lower and these modes become less important.

Gyrokinetic simulations have long been used to simulate the linear and non-linear physics of ITG modes [8]. Most studies have concentrated on large aspect ratio tokamaks where the ratio of ion gyroradius to plasma minor radius ($\rho_* = \rho_\mathrm{i}/a$) is small (for instance in the benchmark study by Dimits, $\rho_* = 1/160$ [9]). At low ρ_* the local treatment of the turbulence is usually sufficient, since the turbulent eddy size created by microinstabilities generally scales with the Larmor radius of the particles driving the instabilities [10]. However, non-local effects on ion scale turbulence are likely to be important in devices where $\rho_{\mathrm{i}*}$ is large. Firstly the equilibrium profiles vary across the radial extent of the turbulent eddies, and secondly turbulence spreading can become important [11, 12]. While the local gyrokinetic flux-tube approximation provides guidance on the linear microstability of ITG and TEM turbulence, in non-linear simulations of ITG turbulence at large $\rho_{\mathrm{i}*}$ a global treatment of the plasma is required for a more quantitative description of the turbulent transport processes.

In the MAST ST, where the toroidal magnetic field at the plasma centre $B \approx 0.5\,\mathrm{T}$ and the ion temperature can exceed 1 keV in the core, the condition of large ρ_* ($\approx 1/50$) is fulfilled. Other important differences with respect to large aspect ratio

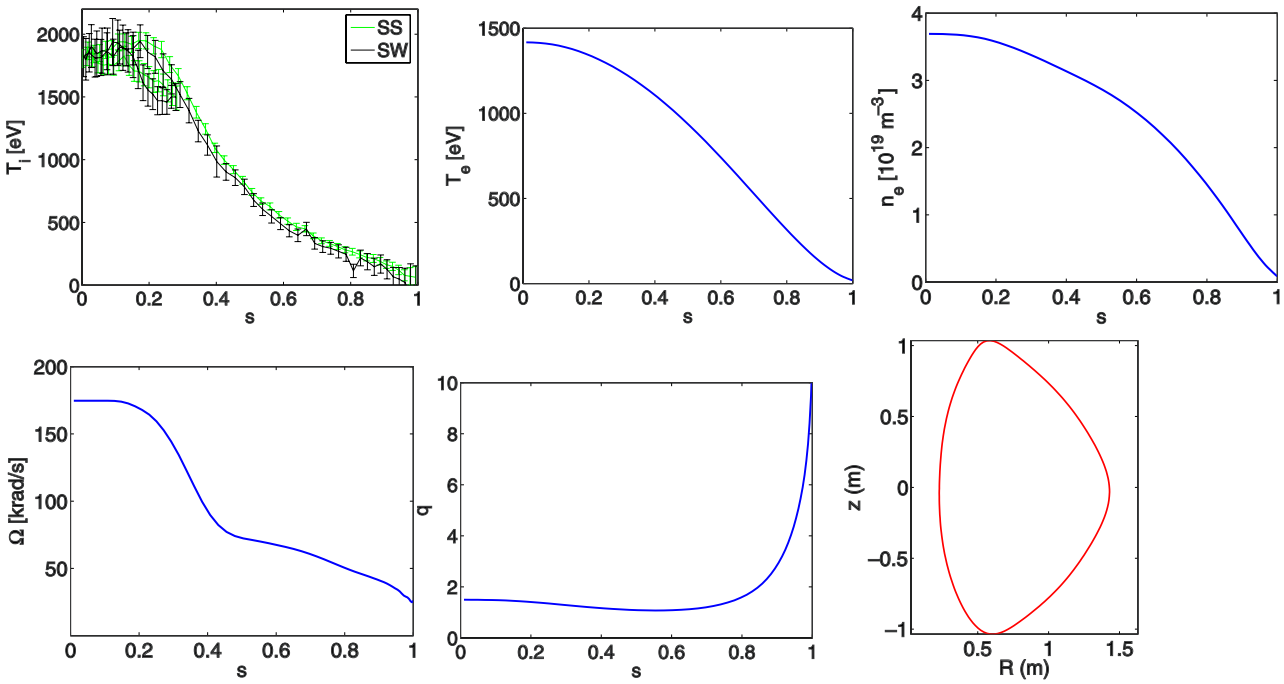

Figure 1. The ion temperature, electron temperature, electron density, toroidal rotation, q-profile and the plasma shape of the MAST discharge #22807 at 0.25 s. The two measurements of ion temperature refer to the two independent neutral beams used by the CXRS system. The inboard side measurements are folded onto the outboard side in $s < 0.3$. The internal transport barrier (ITB) with steep ∇T_i is in the region $0.3 < s < 0.5$.

tokamaks are that MAST has a large trapped particle fraction due to the strong variation of magnetic field inside the plasma, and the MAST core plasma, heated by neutral beams, can reach very high toroidal rotation velocities. This produces a steep flow shear gradient through the plasma. The sheared flow can have a stabilizing effect on the microinstabilities [3–7].

In section 2 of this paper we will describe the MAST experimental equilibrium that is used in the gyrokinetic simulations. In section 3 we will present linear microstability results for ITG and TEM from local and global gyrokinetic codes. In section 4 we will show results of global non-linear simulations of ITG and TEM turbulence in MAST. Furthermore, we show how the flow shear affects the turbulence.

2. Experimental plasma

The plasma studied is taken from the MAST L-mode discharge #22807 [6] at $t = 0.25$ s, with the following global parameters: plasma current $I_\mathrm{p} = 0.88$ MA; toroidal magnetic field B_T (at $R = 1$ m) $= 0.41$ T; and NBI heating in the co-current direction $P_\mathrm{NBI} = 3.3$ MW. Figure 1 shows the ion temperature and toroidal flow profile from charge-exchange recombination spectroscopy (CXRS), the q-profile from MSE-constrained equilibrium reconstruction and the plasma shape. The Mach number of the toroidal flow, $M_\phi = R\Omega/v_\mathrm{ti}$, where Ω is the toroidal rotation, R is the major radius and v_ti is the ion thermal velocity, is in the range $0.4 < M_\phi < 0.5$ throughout the plasma. Steep gradients in ion temperature and toroidal rotation coincide at a transport barrier in the radial region $0.2 < s < 0.4$ [6], where s is the square root of the normalized poloidal flux. There is negative magnetic shear in the core region, $s < 0.55$. In the outer part of the plasma, both the ITG and the toroidal flow shear are significantly smaller than in the core. The value of $\rho_{\mathrm{i}*}$ at $s = 0.5$ is 0.018. We will show later that this $\rho_{\mathrm{i}*}$ is large enough for the global effects become important.

The experimental ion heat flux is determined from power balance using the TRANSP code [13]. The ion neoclassical heat flux, and the contributions due to the time variation of the equilibrium profiles and ion heat sources including the collisional heat exchange between electrons and ions are subtracted from the total ion heat flux to leave as a residual the anomalous heat flux. Unfortunately, even though the input neutral beam power is well known and it is possible to calculate the heat deposition from the fast ions based on particle orbits and collisions, the heat source distribution inside the plasma has uncertainties associated with physics processes that redistribute the fast ions [6]. The fast-ion diffusion is enhanced from the neoclassical level by core plasma MHD activity, especially fishbones and toroidal ripple. These processes are modelled in TRANSP by including anomalous fast-ion diffusion, and adjusting the diffusion coefficient to match the neutron rate. In this particular discharge, the anomalous ion heat flux was well determined without the need to assume anomalous diffusion of fast ions only for times before the second heating beam was turned on at $t = 0.22$ s.

Local linear gyrokinetic simulations have demonstrated that in the plasma region just outside the transport barrier in this equilibrium, ITG/TEM modes at $k_\theta \rho_\mathrm{i} < 1$ (k_θ is the poloidal wavenumber $\sim nq$, where n is the toroidal mode number and q is the safety factor) are not fully stabilized by the relatively

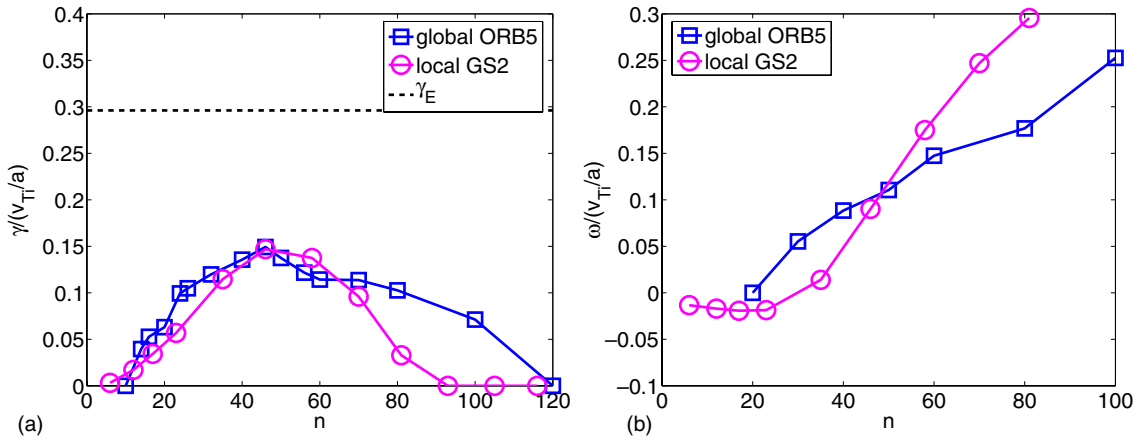

Figure 2. Linear spectra of ITG mode growth rates (*a*) and frequencies (*b*) from electrostatic gyrokinetic simulations with an adiabatic electron response using local flux-tube code GS2 (magenta) and global code ORB5 (blue). The horizontal dashed line shows the level of flow shear in the experiment on the flux surface where the linear analysis was conducted. In the frequency plot the positive values refer to modes propagating in the ion diamagnetic direction.

weak sheared toroidal flow in this part of the plasma [6]. In this paper we perform global gyrokinetic simulations to model the possible impact of the surviving long wavelength modes on anomalous ion heat transport.

3. Linear gyrokinetic simulations

Before presenting non-linear turbulence simulations, we show results from linear plasma microstability calculations using two different electrostatic gyrokinetic codes: the local gyrokinetic flux-tube code GS2 [14]; and the global code ORB5 [15, 16]. This comparison was to assess the importance of non-local effects. Simulations have been carried out with adiabatic electrons and with kinetic trapped electrons, both with and without sheared toroidal equilibrium flows. The linear static ORB5 simulations shown here were performed using 4×10^6 markers on a $N_s \times N_\chi \times N_\phi = 50 \times 512 \times 256$ (where s is the radial, χ is the in-flux-surface direction perpendicular to the magnetic field and ϕ is the toroidal angle). The growth rate for each toroidal mode was calculated with a separate simulation. The simulations with flow used the same grid but more markers (1.6×10^7) were needed for convergence at high flow rates.

3.1. Adiabatic electrons

A global linear run of ORB5 is used to determine the most unstable part of the plasma, i.e. where the growth rate of the linear mode is largest. Further simulations using annular regions of plasma that exclude the most unstable part are used to determine if other regions are unstable. In simulations with adiabatic electrons we find the core is stable to ITG modes, even though the maximum of $\nabla T_\mathrm{i}/T_\mathrm{i}$ occurs in this region ($s < 0.5$). Magnetic shear, $\hat{s} = (r/q)\,\mathrm{d}q/\mathrm{d}r$, is reversed in the core, which can explain the good stability [23]. The most unstable region in this plasma lies between $0.6 < s < 0.8$.

Figure 2 compares dominant linear growth rate spectra from ORB5 and GS2 gyrokinetic simulations with adiabatic electrons for the MAST equilibrium surface at $s = 0.73$. Although there is some disagreement at short and long wavelengths, from the good agreement for the most unstable part of the spectrum we can see that the flux-tube approach is sufficient for this linear analysis. One reason for the disagreement is that in the global simulation, the linear mode is free to peak in the most unstable radial location, while in the local simulation the radial location is fixed. The most unstable part of the spectrum agrees well because the local simulation was conducted on the flux surface where the fastest growing global mode peaks, but at other wavelengths the agreement is not as good because the centre of the global mode is no longer on exactly the same surface as the local one.

To gain further insight into the validity of the local simulations, we have varied ρ_* in the ORB5 simulations. Figure 3 shows how the linear growth rate of the most unstable mode varies with the ρ_* parameter. Global effects start to impact the linear growth rate just below the experimental value of ρ_* of this MAST discharge (=0.018). This agrees well with the result obtained by Lin for large aspect ratio tokamaks [18] and with previous ORB5 results for circular plasmas [19].

The plasma flow can have a significant effect on the microturbulence, both on the linear growth of the modes and on the non-linear effects. A short description of the implementation of the MAST toroidal flow in ORB5 is given in the appendix. A more thorough discussion of the implementation is given in [20]. The shearing rate is defined as [3]:

$$\gamma_E = \frac{r}{q}\frac{\mathrm{d}}{\mathrm{d}r}\left(\frac{q v_{E\times B}}{r}\right), \tag{1}$$

with

$$v_{E\times B} = v_\perp, \tag{2}$$

where $v_\perp$ is the velocity component perpendicular to the magnetic field and it is calculated using the toroidal rotation rate Ω profile and the equilibrium magnetic field line.

To study the stabilizing effect of the flow, we apply radially constant flow shear (γ_E) across the plasma and vary its amplitude. We find that the stabilizing effect is slightly asymmetrical with respect to the direction of the flow shear

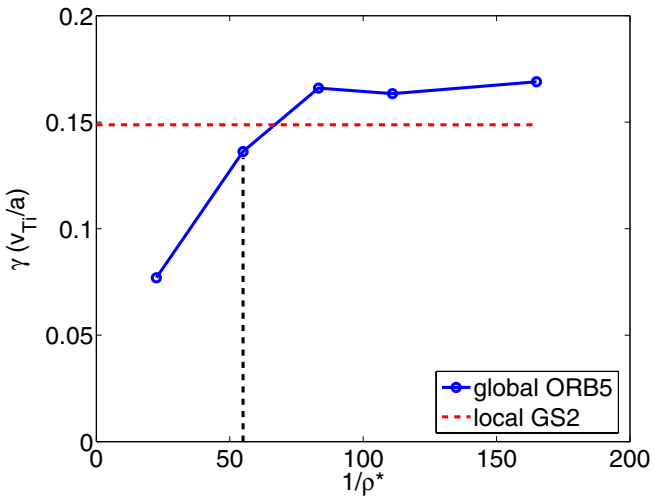

Figure 3. The growth rate of $n = 50$ mode as a function of $1/\rho_*$. The vertical line represents the experimental value. The horizontal line represents the local flux-tube result obtained using GS2.

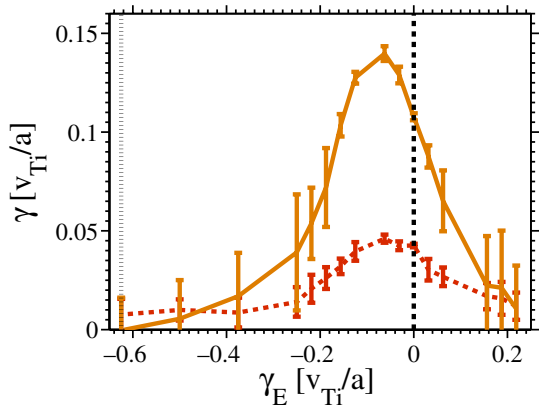

Figure 4. The growth rates of $n = 60$ (solid orange) and $n = 20$ (dashed red) ITG modes as a function of the assumed profile of toroidal flow. The negative values represent core rotation in the co-direction with the plasma current and positive values counter-direction. The experimental value of flow shear ($0.61\ v_{T_i}/a$) is indicated by a dotted line. The error bars represent the uncertainty of the growth rates obtained using linear fitting similar to figure 5(*b*).

(figure 4). If the flow is in the co-current direction and the flow profile is monotonically decreasing from the core, a small sheared toroidal flow actually destabilizes the ITG mode. If the gradient of the flow at the surface of interest is reversed (e.g. by reversing the flow everywhere, or alternatively by reversing the flow gradient locally), then any finite flow becomes stabilizing. The physical explanation for the asymmetry is given in [21]: depending on the relative signs of the radial shear in the drift wave eigenfrequency and the radial shear in the toroidal rotation, a small flow shear either compensates for the mode tilting due to the diamagnetic shear to destabilize the mode, or enhances this tilting to stabilize the mode. Large flow shears always dominate the shear in the eigenfrequency and are always stabilizing.

In order to fully stabilize the ITG modes we find that γ_E has to be much more than 2 times the growth rate of the mode. The most unstable modes are stabilized more effectively than those with long wavelength making the spectrum almost flat at the experimental level of flow shear. It must be noted that all the growth rates at the experimental level of flow shear are very small $<0.01 v_{T_i}/a$. A possible reason for the weaker stabilization at long wavelengths is the aspect ratio of radial to poloidal width of the mode. The fastest growing mode in a static case has more radially elongated mode structure than the longer wavelength modes making them easier to stabilize by sheared flow. More discussion about this effect is found in [22].

Figure 5 shows how the growth rates, with and without the experimental flow, vary as a function of the assumed ITG. Here instead of the experimental temperature profile we have used a parametrized temperature profile that has its peak gradient at $s = 0.5$ and have varied the gradient length (R/L_T). The radial profile shape of the temperature gradient used in the scan is shown in figure 5(*c*). Without flow shear effects the plasma would be unstable to ITG modes even below the experimental ITG, but figure 5(*b*) shows the growth of the mode in the case of experimental gradients with flow, demonstrating that sheared flow makes the experimental plasma very close to marginal stability for ITG modes.

3.2. *Kinetic trapped electrons*

The trapping fraction is roughly proportional to the square root of the inverse aspect ratio, giving rise to more trapped particles in a ST than in a large aspect ratio tokamak. While the passing electrons can be assumed to respond adiabatically to the perturbed electric field from low-n modes, the kinetic trapped electrons can contribute to the ITG mode drive and can drive trapped electron modes [12, 17]. In the ORB5 kinetic trapped electron model, only the trapped electrons are treated kinetically and the passing electrons follow the adiabatic response.

Figure 6 shows linear growth rates of the ion scale modes using a kinetic trapped electron model. These are higher than the adiabatic electron results given in figure 2. In the absence of collisions, the global ORB5 growth rates and real frequencies agree reasonably well with the GS2 flux-tube result. Including the collisions in GS2 reduces the growth rates, but they still exceed both the ITG growth rates with adiabatic electrons, and the experimental flow shear rate.

Including flow shear effects in simulations with kinetic trapped electrons, the growth rates stay well above zero, unlike in the case with adiabatic electron response. Local GS2 simulations have also demonstrated that sheared flow does not fully suppress ion scale instabilities in the outer regions of this MAST plasma [6]. The kinetic treatment of electrons does not alter the asymmetry of growth rates with respect to the direction of the flow shear.

4. Global non-linear gyrokinetic simulations

While the linear analysis can be used to study the stability of the plasma, only non-linear simulations can be used to estimate the transport rate of energy and particles that the turbulence produces. ORB5 minimizes the problem of noise using a $k_\parallel$ filter to eliminate unphysical modes, and a relaxation operator

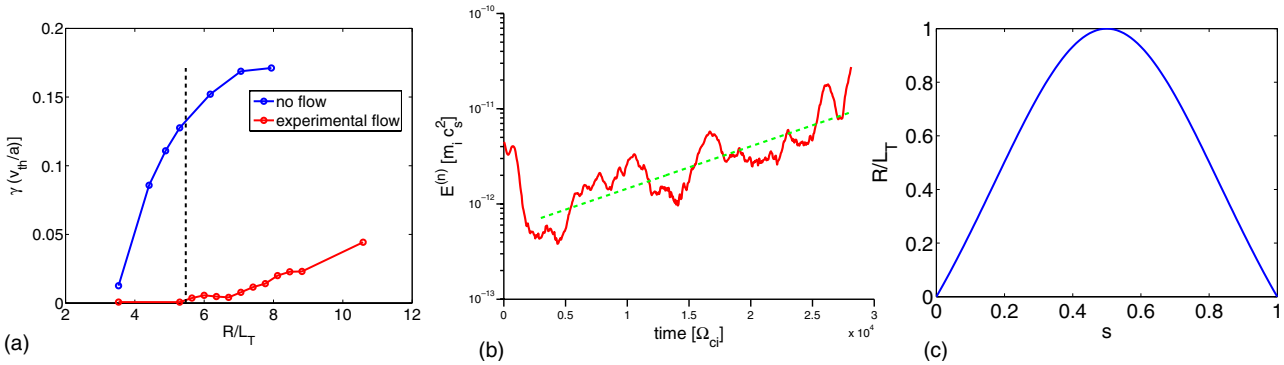

Figure 5. (a) The growth rate of the most unstable ITG mode as a function of normalized ITG R/L_T for ORB5 simulations with and without the experimental flow. The vertical line shows the experimental ITG at $s = 0.5$. The growth rates with flow are averaged over fluctuations in the plot of energy in the perturbation as a function of the simulation time, as shown in (b) for the case with experimental gradients.

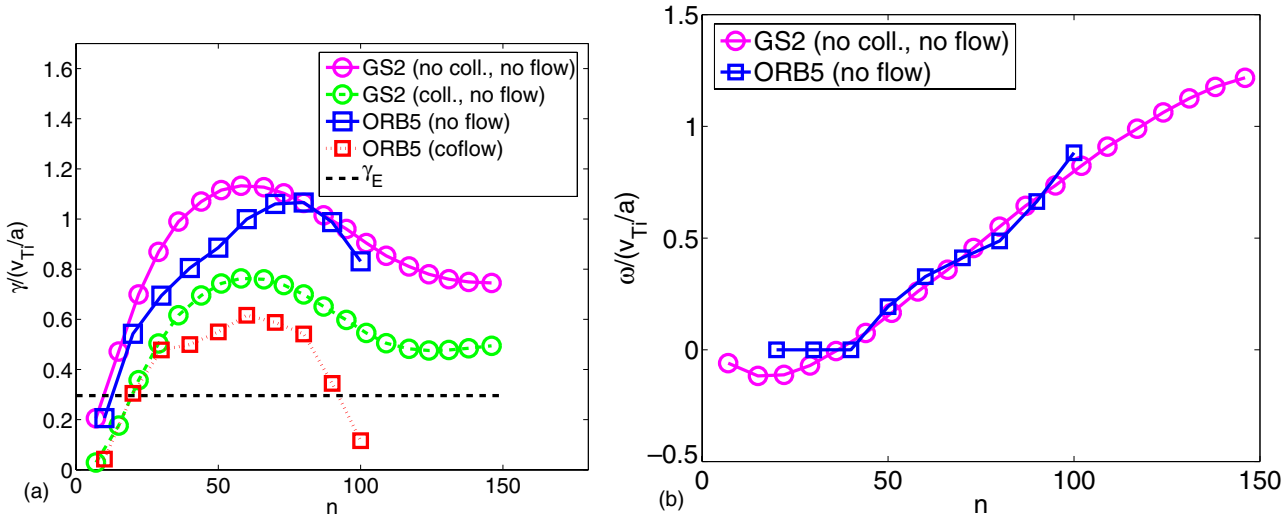

Figure 6. Linear growth rate (a) and real frequency (b) spectra from simulations with kinetic trapped electrons using local flux-tube code GS2 with no flow and no collisions (magenta circles), no flow and collisions (green circles), and global code ORB5 without collisions and no flow (blue squares) and experimental flow in the co-direction (red squares). The GS2 simulations are performed on flux surface $s = 0.76$ where the ORB5 mode is found to peak. The plotted experimental flow shear (γ_E) is evaluated on this surface as well. Real frequencies are shown only for simulations without flow or collisions.

to ensure that the marker weights stay bounded but taking care not to impact on the zonal flow dynamics [15, 24]. A heating operator is also used to keep temperature profiles from relaxing during the simulation. The heating operator does not try to simulate the experimental heating profile, but only pushes the perturbed profiles towards the initial equilibrium profiles [24].

4.1. Adiabatic electrons without sheared flow

The non-linear ORB5 simulations are performed using 2×10^8 markers on a $N_s \times N_\chi \times N_\phi = 50 \times 512 \times 256$ grid (where s is the radial, χ is the in-flux-surface direction perpendicular to the magnetic field and ϕ is the toroidal angle).

Neglecting sheared toroidal flow and using the adiabatic electron response (i.e. neglecting the trapped electron drive), the turbulence moves from the linearly unstable region to the linearly stable region during the non-linear phase. This can be seen in figure 7 where the ion heat flux is plotted as a function of time and radius and in figure 8(a) where ion heat flux at the saturated non-linear state and the maximum local growth rates

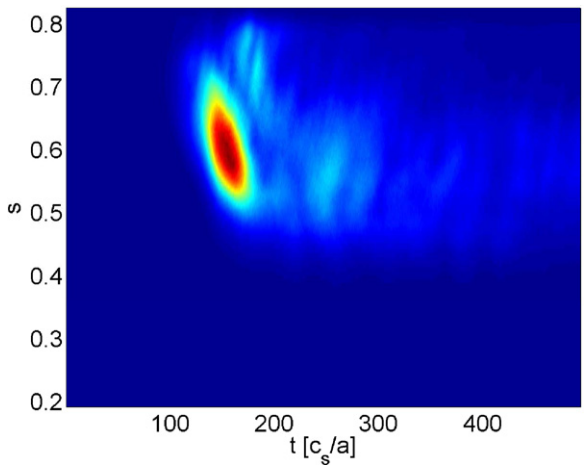

Figure 7. The ion heat flux (in MW m^{-2}) as a function of s and time from an ORB5 simulation using experimental equilibrium profiles, adiabatic electron response and neglecting sheared toroidal flow.

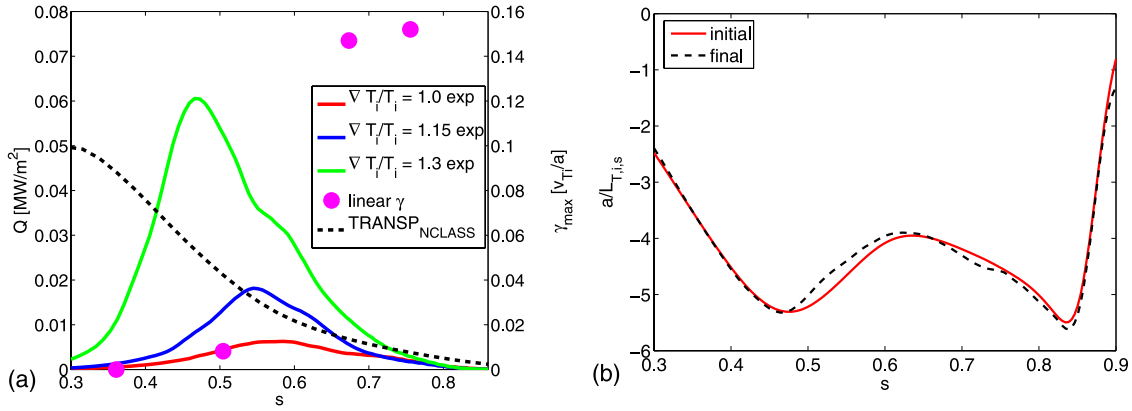

Figure 8. (*a*) The ion heat flux as a function of s in a ORB5 simulation with experimental (red), 15% increased (blue) and 30% increased ITGs. Also plotted is the neoclassical heat flux calculated by TRANSP (dashed line) as well as the region where the mode grows in the linear phase (magenta). (*b*) The normalized ITG length a/L_T in the beginning (solid red) and end (dashed black) of the non-linear simulation with 30% increased ITG. The heat fluxes are time averaged over the last 150 c_s/a of the simulation. The magenta dots represent the maximum values of local growth rates.

calculated by GS2 are shown. The turbulence starts around $s \approx 0.7$ (which was found to be the most linearly unstable region), but then spreads inwards all the way to $s \approx 0.4$. During the saturated phase the maximum amplitude of the heat flux is located between $s = 0.4$ and $s = 0.7$. As can be seen in figure 8(*b*), the ITG changes very little during the simulation due to the heating operator. Therefore, the spreading of turbulence is not due to the steepening of core profiles by the turbulence. The more likely explanation is either the spreading of turbulent eddies from the linearly unstable outer region to the linearly stable core region or the linearly very slowly growing modes in the mid-radius becoming dominant over the fast growing modes in the outer radius during the non-linear phase.

The signal to noise ratio is defined in [16] as the ratio of the physical mode contribution to the charge density to that associated with unphysical modes that should be damped, i.e. whose amplitude is purely due to the noise. It stays above 20 through the simulation. For the grid convergence test, we did runs with twice the number of radial points. The fluxes and non-linear spectrum were unaffected, but the signal to noise ratio was halved.

When we compare the level of turbulent transport created by saturated ITG turbulence (assuming adiabatic electrons), we find that at experimental temperature profiles and even without considering any equilibrium flow shear stabilization, the turbulent heat flux is very low, and below the neoclassical level calculated by NCLASS in TRANSP (figure 8). Increasing the ITG in the core region ($s = 0.3$–0.5) by 30% increases the heat flux well above the neoclassical level. Neglecting sheared toroidal flows it would seem that the plasma ion temperature profile is just below the non-linear threshold for ITG turbulence.

4.2. Kinetic trapped electrons with and without sheared flow

In the non-linear ORB5 simulations with kinetic trapped electrons we assume $m_e/m_i = 0.005$ instead of the physical value of 2.72×10^{-4} for deuterium plasma. This approximation

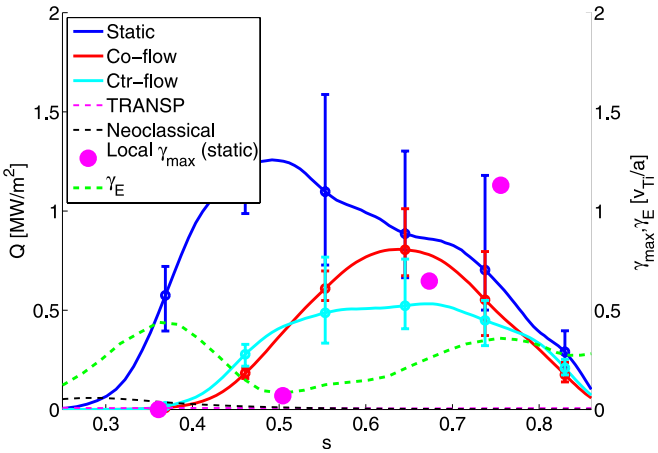

Figure 9. The ion heat flux in ORB5 simulations with kinetic trapped electrons with co-flow (red), counter-flow (cyan) and without flow (blue) as a function of s. The green dashed line shows the γ_E profile and the magenta dots represent the maximum values of local growth rates. Additionally neoclassical (dashed black) and anomalous (magenta) flux calculated by TRANSP is plotted.

saves computing resources. In a linear study we found that the growth rates are not sensitive to the ratio m_e/m_i. The change in the linear growth rate is less than 10% when m_e/m_i is varied by 3 orders of magnitude from the physical value.

As shown in section 3, the linear growth rate becomes much larger when the trapped electrons are treated kinetically. The kinetic treatment also leads to significantly higher ion heat flux in a non-linear simulation. Using the experimental profiles and neglecting sheared flow, the modelled ion heat flux is well above both the neoclassical ion heat flux and the experimental level of anomalous ion heat flux calculated by TRANSP (figure 9). The error bars in figure 9 represent the variation of the heat flux during the saturated non-linear phase. As in the adiabatic electron case, the turbulence extends from the linearly most unstable region (which in this case is even further from the core than in the ITG simulation) towards the core, and the maximum heat flux during the saturated turbulence is in the negative shear region where the linear

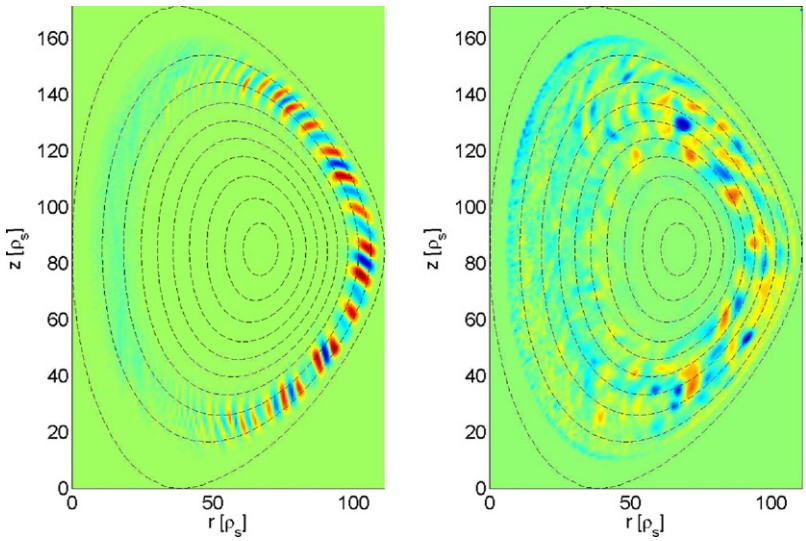

Figure 10. The perturbed potential $\phi - \langle\phi\rangle$ (where $\langle\phi\rangle$ is the flux surface averaged potential) during the linear (left) and fully saturated (right) phase of the ORB5 simulation where trapped electrons were treated kinetically and without flow.

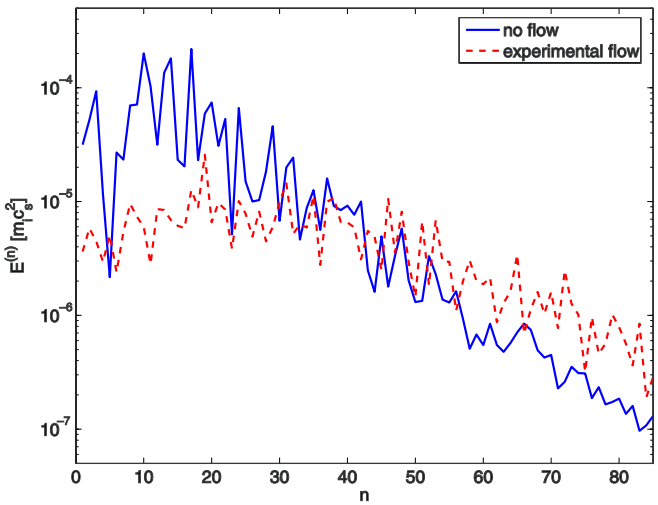

Figure 11. The non-linear energy spectrum (energy of a given toroidal mode) for the ORB5 simulation including the kinetic trapped electrons.

modes are either fully stabilized ($s = 0.4$) or close to marginal stability ($s = 0.5$).

Including sheared flow, the turbulent heat flux remains well above both the neoclassical level and the anomalous level calculated by TRANSP in the outer region ($s > 0.5$). However, the sheared flow was found to reduce the spreading of turbulence into the strong flow shear region ($s < 0.45$). It is also interesting to note that while there is an asymmetry in linear growth rates with respect to the direction of the flow, the non-linear heat flux shows only a weak asymmetry. In both cases, the turbulence spreads inwards up to the location with strong flow shear.

During the non-linear phase of a simulation without flow shear the energy spectrum shifts towards long wavelength modes from the linearly most unstable modes. As shown in figure 11 most of the energy in the non-linear phase is in the modes with $n = 15$, well below the peak in the linear growth rate spectrum ($n = 50$). When the flow shear effects are taken into account, the non-linear shift in the energy spectrum is more modest. Even though linearly the long wavelength modes were affected less by the flow shear than the fastest growing modes, non-linearly the flow shear seems to reduce the reverse cascade of energy into long wavelength modes that is seen in the spectrum of the simulation without flow shear.

The increased size of the turbulent eddies in the non-linear phase can also be seen in figure 10 where the perturbed potential is plotted in a poloidal cross section of the plasma during the linear and non-linear phase.

Since the spectrum changes during the non-linear phase from the linear phase, the turbulence spreading cannot be quantified just by comparing the radial width and position of the most unstable linear mode to the non-linear phase. In figure 12 we compare the radial localization of the non-linear turbulence to two linear analyses. The first is carried out for the most unstable mode in the linear phase ($n = 60$), the second to the mode that is found to have most energy during the non-linear phase ($n = 15$). The difference between the two linear analyses can be interpreted as the widening effect due to change in the turbulence spectrum in the non-linear phase. As can be seen, the mode affected region broadens slightly due to the change in the spectrum, but this effect is relatively small compared with the non-linear turbulence extension into the core during the non-linear phase.

Since it is difficult to map out linearly stable regions using a global code, we have also performed linear local gyrokinetic runs in the negative shear region using GS2 with kinetic electrons and without flow at $s = 0.36$ and $s = 0.50$. The GS2 runs found either no unstable ion scale modes ($s = 0.36$) or modes with very low growth rates ($s = 0.50$). The stable surface is shown with a vertical line in figure 12.

This indicates that the region that is affected by the turbulence during the non-linear phase extends deep into the core region and that this is not due to the change in the spectrum. This turbulence broadening effect is observed in our global simulations with sheared flow. Even then the turbulent

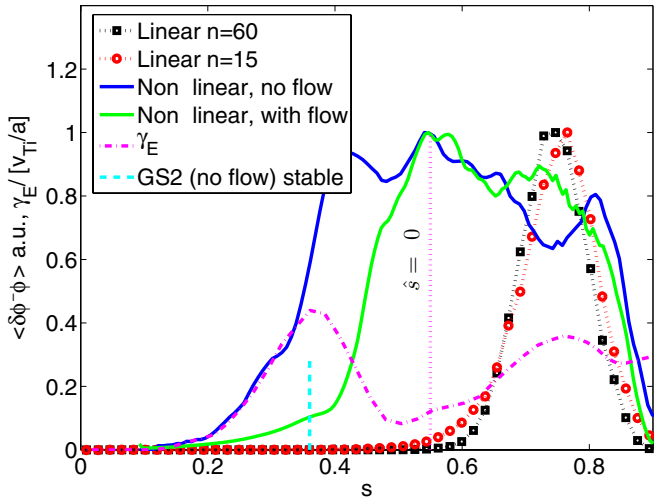

Figure 12. The flux surface average of the normalized potential fluctuation amplitude in the non-linear phase of the simulation with (solid green) and without flow (solid blue) and in a linear simulation for the mode with the largest linear growth rate (black squares), the mode with most energy in a non-linear simulation without flow (red circles). The simulation is performed with kinetic trapped electrons. The vertical dashed lines show the shear reversal point (magenta) and the flux surface that was found stable (dashed cyan) in a local GS2 simulation with no flow. The profile of γ_E is plotted in dashed–dotted magenta.

region extends towards the core, but in that case the spreading is limited by the steep flow gradient in the core ($s < 0.45$).

Local simulations indicate that collisions reduce the trapped electron drive, and this effect may also reduce the non-linear flux in the outer region of the plasma. Gyrokinetic studies have found that collisions can reduce the linear drive [3] and transport driven by trapped electrons [26]. On the other hand, the collisions may increase the ITG fluxes by damping zonal flows [27]. We plan to study the effect of collisions on MAST turbulence in future global simulations with ORB5.

5. Conclusions

Gyrokinetic modelling of ion scale turbulence in MAST L-mode plasma, with $\rho_* = 0.018$, shows clear non-local behaviour. While the linear growth rate spectrum agrees well with the local flux-tube analysis, the non-linearly saturated state of the turbulence can be modelled most reliably in global simulations. In global gyrokinetic simulations where sheared toroidal equilibrium flows are neglected, we find that in the non-linear phase the turbulence extends to the core regions that have either very slowly growing linear modes or are fully stable. In the saturated non-linear turbulent phase the maximum heat flux has moved from the linearly most unstable outer region into the core.

At low γ_E, flow shear has an asymmetric effect on linear ITG stability with respect to the direction of the sheared toroidal flow. Monotonically decreasing flow in the co-direction is destabilizing at low flow shear, but stabilizing at high flow shear. Monotonically decreasing counter-flow is found to be stabilizing for all flow shearing rates. At the experimental level of flow shear, the MAST plasma is close to the linear stability boundary for ITG modes when electrons are treated adiabatically. Adding kinetic trapped electrons in the simulations increases the growth rates and results in unstable modes even when experimental flow shear is taken into account. Additionally the flow shear shifts the peak of the linear growth rate spectrum towards long wavelength modes by having a stronger stabilizing effect on short wavelength modes. In non-linear simulations with flow shear effects taken into account we still find the turbulence spreading into the linearly stable region, but due to the strong experimental flow shear in the core region it does not expand as deep into the core as in the static case.

The level of turbulent heat flux from ion scale turbulence in this MAST plasma is sensitive to the electron response and the inclusion of sheared toroidal equilibrium flow. Global gyrokinetic calculations have been performed using ORB5, including kinetic trapped electron physics which drives turbulence, and sheared flow which is generally stabilizing. Such simulations predict a level of ion heat flux that significantly exceeds ion neoclassical heat flux in the outer region of this MAST plasma. In the future we look forward to comparing beam emission spectroscopy measurements of ion scale turbulence in MAST with simulations [25]. Also in the future, the effect of collisions on the non-linear turbulence will be investigated further.

Acknowledgments

This work was funded by the RCUK Energy Programme under grant EP/I501045 and the European Communities under the contract of Association between EURATOM and CCFE. The views and opinions expressed herein do not necessarily reflect those of the European Commission. The computations were carried out using HECToR (grant number EP/H002081/1) and HPC-FF supercomputers.

Appendix. Flow shear implementation in ORB5

Equilibrium flow shear has been included in ORB5 with a background radial electric field and a shifted Maxwellian distribution function for the equilibrium distribution function, f_0:

$$f_0 = \frac{n_0(\psi_c)}{(2\pi T(\psi_c)/m)^{3/2}} \exp\left(-\frac{\epsilon - q\phi_0(\psi_*)}{T(\psi_c)}\right), \qquad (A.1)$$

where m, q, T and n_0 are the mass, charge, temperature and density, $\epsilon = mv^2/2 + q\phi_0(\psi)$ is the energy, ψ is the poloidal magnetic flux, $\psi_c = mv_{||}RB_\zeta/qB$ is the canonical momentum and ψ_* is the modified canonical momentum that is used to vary the flow from pure toroidal to pure poloidal flow [20]. The electric potential ϕ_0 is calculated by integrating the radial electric field set by

$$E_r = (Zen)^{-1}\nabla p - \boldsymbol{v} \times \boldsymbol{B}, \qquad (A.2)$$

where p is the pressure, $\boldsymbol{v}$ is the velocity of the plasma and $\boldsymbol{B}$ is the magnetic field. The toroidal flow velocity v_ϕ on the outboard side of the plasma is obtained from the charge exchange diagnostic and the poloidal magnetic field B_θ from

the equilibrium reconstruction. Here we consider only toroidal flows, since flow shear can only compete with growth rates if flows are sonic, and therefore toroidal.

Choosing canonical momentum, $\psi_* = \psi_c$, gives almost pure toroidal flow because the poloidal flow from $E_0 \times B$ cancels the poloidal component of the parallel flow. Since we consider small background flows $v_{\text{flow}}/v_{\text{th}} \ll 1$, we can use normal gyrokinetic equations of motion with $E_0 + \langle E_1 \rangle$ replacing the usual terms with $\langle E_1 \rangle$. More details of the procedure can be found [20].

References

[1] Kaye S M *et al* 2007 *Nucl. Fusion* **47** 499
[2] Roach C M *et al* 2005 *Plasma Phys. Control. Fusion* **47** B323
[3] Roach C M *et al* 2009 *Plasma Phys Control. Fusion* **51** 124020
[4] Guttenfelder W *et al* 2012 *Phys. Plasmas* **19** 022506
[5] Field A R *et al* 2004 Core heat transport in the MAST spherical tokamak *Proc. 20th IAEA Fusion Energy Conf. (Vilamoura, Portugal, 2004)* EX/P2-11
[6] Field A R *et al* 2011 *Nucl. Fusion* **51** 063006
[7] Waltz R E, Kerbel G D and Milovich J 1994 *Phys. Plasmas* **1** 2229
[8] Parker S E *et al* 1993 *Phys. Rev. Lett.* **71** 2042
[9] Dimits A M *et al* 2000 *Phys. Plasmas* **7** 969
[10] Candy J, Waltz R E and Dorland W 2004 *Phys. Plasmas* **5** L25
[11] Lin Z and Hahm T S 2004 *Phys. Plasmas* **11** 1099
[12] Sydora R D, Decyk V K and Dawson J M 1996 *Plasma Phys. Control. Fusion* **38** A281
[13] Goldston R J *et al* 1981 *J. Comput. Phys.* **43** 61
[14] Kotschenreuther M, Rewoldt G and Tang W M 1995 *Comput. Phys. Commun.* **88** 128
[15] Jolliet S *et al* 2008 *Comput. Phys. Commun.* **177** 409
[16] Bottino A 2007 *Phys. Plasmas* **14** 010701
[17] Dannert T and Jenko F 2005 *Phys. Plasmas* **12** 072309
[18] Lin Z, Ethier S, Hahm T S and Tang W M 2002 *Phys. Rev. Lett.* **88** 195004
[19] McMillan B F *et al* 2010 *Phys. Rev. Lett.* **105** 155001
[20] McMillan B F *et al* 2011 *Phys Plasmas* **18** 112503
[21] Kishimoto Y *et al* 1999 *Plasma Phys. Control. Fusion* **41** A663
[22] Hill P *et al Plasma Phys. Control. Fusion* submitted
[23] Drake J F *et al* 1996 *Phys. Rev. Lett.* **77** 494
[24] McMillan B F *et al* 2008 *Phys. Plasmas* **15** 052308
[25] Field A R *et al* 2012 *Rev. Sci. Instrum.* **83** 013508
[26] Romanelli M *et al* 2011 *Nucl. Fusion* **51** 103008
[27] Vernay T *et al* 2010 *J. Phys.: Conf. Ser.* **260** 012021